DOI: 10.1002/chem.200601152

Osmium(II) and Ruthenium(II) Arene Maltolato Complexes: Rapid Hydrolysis and Nucleobase Binding

Anna F. A. Peacock,[a] Michael Melchart,[a] Robert J. Deeth,[b] Abraha Habtemariam,[a] Simon Parsons,[a] and Peter J. Sadler*[a]

Abstract: Density functional calculations show that aquation of $[Os(\eta^6\text{-arene})(XY)Cl]^{n+}$ complexes is more facile for complexes in which XY = an anionic O,O-chelated ligand compared to a neutral N,N-chelated ligand, and the mechanism more dissociative in character. The O,O-chelated XY = maltolato (mal) $[M(\eta^6\text{-}p\text{-cym})(mal)Cl]$ complexes, in which *p*-cym = *p*-cymene, M = Os^{II} (**1**) and Ru^{II} (**2**), were synthesised and the X-ray crystal structures of **1** and **2**·2 H_2O determined. Their hydrolysis rates were rapid (too fast to follow by NMR spectroscopy). The aqua adduct of the Os^{II} complex **1** was 1.6 pK_a units more acidic than that of the Ru^{II} complex **2**. Dynamic NMR studies suggested that O,O-chelate ring opening occurs on a millisecond timescale in coordinating proton-donor solvents, and loss of chelated mal in aqueous solution led to the formation of the hydroxo-bridged dimers $[(\eta^6\text{-}p\text{-cym})M(\mu\text{-}OH)_3M(\eta^6\text{-}p\text{-cym})]^+$. The proportion of this dimer in solutions of the Os^{II} complex **1** increased with dilution and it predominated at micromolar concentrations, even in the presence of 0.1 M NaCl (conditions close to those used for cytotoxicity testing). Although 9-ethylguanine (9-EtG) binds rapidly to Os^{II} in **1** and more strongly ($\log K$ = 4.4) than to Ru^{II} in **2** ($\log K$ = 3.9), the Os^{II} adduct $[Os(\eta^6\text{-}p\text{-cym})(mal)(9EtG)]^+$ was unstable with respect to formation of the hydroxo-bridged dimer at micromolar concentrations. Such insights into the aqueous solution chemistry of metal–arene complexes under biologically relevant conditions will aid the rational design of organometallic anticancer agents.

Keywords: bioinorganic chemistry · density functional calculations · O ligands · osmium · ruthenium

Introduction

Third-row transition-metal ions are commonly considered to be more inert than those of the first and second rows. For example, substitution reactions of third-row Pt^{II} complexes are commonly approximately five orders of magnitude slower than those of their second-row Pd^{II} analogues.[1a] Similarly, osmium(II) and (III) complexes are often kinetically more inert than their Ru analogues.[1]

There is current interest in reactions of Ru^{II}–arene complexes containing N,N- or O,O-chelating ligands that exhibit cytotoxicity towards cancer cells.[2–6] However, there are few reports of the aqueous chemistry of Os^{II}–arene complexes,[7–9] especially under biologically relevant conditions and concentrations. Recently, we have shown that the anionic O,O-chelating ligand, XY = acetylacetonato (acac), in arene complexes $[Os(\eta^6\text{-arene})(XY)Cl]^{n+}$ can dramatically increase the reactivity of the Os^{II}–Cl bond compared to, for example, complexes with the neutral N,N-chelating ligand XY = ethylenediamine (en).[10,11] Here, we compare the chemistry of an Os^{II}–*p*-cymene complex containing the potentially more stable five-membered chelate ring of maltolate (mal; 3-oxy-2-methyl-4-pyrone) with its Ru^{II} analogue. Maltol is a natural product, a food additive with low cytoxicity, but it exhibits antitumour activity in some neuroblastoma cell lines.[12] Complexes of maltolate chelated to metals have been investigated for the treatment of some diseases.[13] The most extensively studied are bis(maltolato)oxovanadium(IV) and bis(ethylmaltolato)oxovanadium(IV), which are insulin-enhancing, antidiabetic agents.[14,15] Aluminium(III)–maltolato complexes are known to enhance the toxicity of

[a] A. F. A. Peacock, Dr. M. Melchart, Dr. A. Habtemariam, Dr. S. Parsons, Prof. Dr. P. J. Sadler
School of Chemistry
University of Edinburgh
West Mains Road, Edinburgh EH9 3JJ (UK)
Fax: (+44) 131-650-6453
E-mail: P.J.Sadler@ed.ac.uk

[b] Dr. R. J. Deeth
Department of Chemistry
University of Warwick
Coventry CV4 7AL (UK)

Supporting information for this article is available on the WWW under http://www.chemeurj.org/ or from the author.

aluminium in neuronal cells.[16] Gallium(III) tris(maltolate) is on clinical trial as an anticancer agent,[17] and has potential as a radiopharmaceutical,[18] and ferric tris(maltolate) has been investigated for the treatment of iron-deficiency anaemia.[19,20] Some reactions of Ru^{II}–arene complexes containing maltolate and similar ligands, for example, ethylmaltolate, have been reported,[21–24] but not those of their Os^{II} arene analogues.

We have used density functional calculations to compare the aquation pathways for [Os(η^6-*p*-cym)(acac)Cl] and [Os(η^6-biphenyl)(en)Cl]$^+$, and studied the hydrolysis of [M(η^6-*p*-cym)(mal)Cl] complexes, in which M = Os^{II} (**1**) and Ru^{II} (**2**) containing O,O-chelated maltolate, as well as the acidity of their aqua adducts. Their rates of reaction with guanine and adenine derivatives, and the stabilities of the resulting nucleobase adducts were investigated. Particular emphasis is placed on studies under biologically relevant conditions, especially at micromolar concentrations similar to those used in cell cytotoxicity tests. The behaviour of the O,O-chelated Os^{II}–arene complexes under these conditions is surprising and is discussed in relation to their lack of biological activity.

Results

Aquation pathways: The pathways for aquation of N,N- and O,O-chelated Os^{II} complexes were first compared by using density functional calculations. A preliminary test of the structural accuracy of the Perdew–Wang functional[25] PW91 was performed by comparing the fully optimised in vacuo structure of [Os(η^6-biphenyl)(en)Cl]$^+$ (**13**) with the X-ray crystal structure of the tetraphenylborate salt. PW91 generally overestimates the Os–L (L = ligand) contacts by around 0.03 to 0.04 Å, although the calculated and observed Os–Cl distances are equal at 2.40 Å. The computed structure has the coordinated aryl group twisted slightly, while the "free" aryl group rotates out of the plane of the coordinated ring by about 30°. Conductorlike screening model (COSMO) solvation[26] decreases the twist of the "free" aryl group significantly and brings the coordinated aryl group closer, in better agreement with the experimental distances. The calculated Os–Cl distance lengthens to 2.46 Å but, overall, the agreement with experiment is good (see Figure S1).

The aquation pathway was first explored by means of a series of linear transit calculations to map out the potential energy surface as a function of the Os–Cl and Os–OH_2 distances. Plots for the [Os(η^6-*p*-cym)(acac)Cl] complex (**11**) and [Os(η^6-biphenyl)(en)Cl]$^+$ complex (**13**) are shown in Figure 1. These plots were used to locate an approximate starting point for a full transition-state optimisation. The relevant Os–ligand distances for reactant, transition state and product are given in Table 1 and the associated structures are shown in Figure 2. The reactions modelled are as shown in Equations (1) and (2):

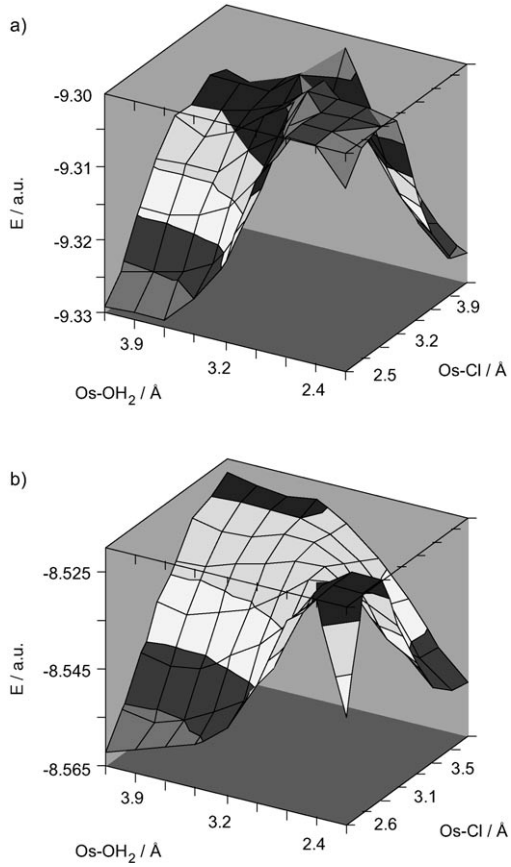

Figure 1. Reaction potential-energy surfaces for the hydrolysis of a) [Os(η^6-*p*-cym)(acac)Cl] (**11**) and b) [Os(η^6-biphenyl)(en)Cl]$^+$ (**13**).

Table 1. Calculated reaction energies ΔE and Os–ligand distances for reactant, transition state (TS) and product for the aquation of [Os(η^6-*p*-cym)(acac)Cl] (**11**) and [Os(η^6-biphenyl)(en)Cl]$^+$ (**13**).

	acac			en		
	ΔE [kJ mol^{-1}]	Os–Cl [Å]	Os–O [Å]	ΔE [kJ mol^{-1}]	Os–Cl [Å]	Os–O [Å]
reactant	0	2.46	4.10	0	2.46	4.28
TS	61	4.21	3.51	90	3.40	3.08
product	9	4.35	2.20	29	4.43	2.14

$$[Os(arene)(acac)Cl] \cdot H_2O \rightarrow [TS] \rightarrow [Os(arene)(acac)(OH_2)]^+ \cdot Cl^- \quad (1)$$

$$[Os(arene)(en)Cl]^+ \cdot H_2O \rightarrow [TS] \rightarrow [Os(arene)(en)(OH_2)]^{2+} \cdot Cl^- \quad (2)$$

The system retains the entering and leaving group within the second coordination sphere as appropriate. This substitution process can be described in terms of two parameters: the Os–Cl and Os–OH_2 distances. In principle, the process could be described as associative or dissociative. The reaction with XY = acac is appreciably more dissociative than for XY = en. It is notable that the water ligand has to reor-

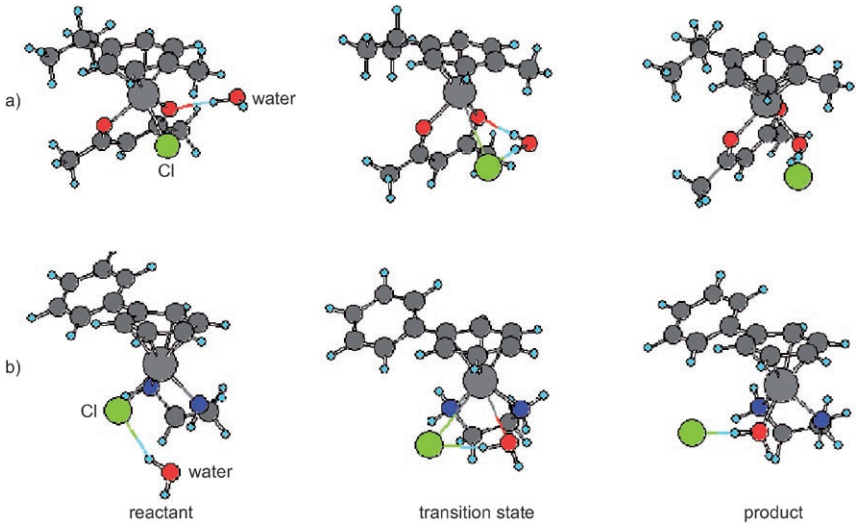

Figure 2. Calculated structures of the reactant, transition state (TS) and product for the hydrolysis of a) [Os(η⁶-*p*-cym)(acac)Cl] (**11**) and b) [Os(η⁶-biphenyl)(en)Cl]⁺ (**13**).

ganise itself from TS to product. For XY = en, an amine hydrogen atom forms an H-bond with the water oxygen atom, thereby allowing the water ligand to orient itself for Os–O bond formation. For XY = acac, the acac oxygen atoms are now H-bond acceptors and the water oxygen atom points away from Os in the transition state. Nevertheless, the overall process is predicted to be significantly more facile for XY = acac than for XY = en, both in terms of a lower barrier (nearly 30 kJ mol^{-1}) and lower exothermicity (note that entropy is not included here).

Preparation and structures of maltolato complexes: The metal–arene–maltolato complexes [M(η⁶-*p*-cym)(mal)Cl], in which M = Os (**1**) and M = Ru (**2**) were prepared in good yields by reaction of the chloro-bridged dimers [M(η⁶-*p*-cym)(Cl)$_2$]$_2$ with the five-membered O,O-chelating ligand maltolate, a route similar to that reported for [Ru(η⁶-mes)(etmal)Cl] (mes = 1,3,5-trimethylbenzene; etmal = ethyl maltolate).[21]

We determined the X-ray crystal structures of [Os(η⁶-*p*-cym)(mal)Cl] (**1**) and the Ru analogue, which crystallised as the hydrated [Ru(η⁶-*p*-cym)(mal)Cl]·2H$_2$O (**2**·2H$_2$O; Figures 3a and b, respectively). Crystallographic data and bond lengths and angles are listed in Tables 2 and 3. Both complexes adopt the pseudo-octahedral "three-leg piano stool" geometry, with the metal π-bonded to the *p*-cymene ring (the "seat") and σ-bonded to a chloride and two oxygen atoms of the chelated maltolate ligand (the "legs"). The M–Cl bond distances are similar for the two metals (2.4326(16) Å for **1** and 2.4329(5) Å for **2**). Coordinated maltolate is unsymmetrical with the two metal–oxygen bond distances being non-equivalent: 2.114(4) and 2.091(5) Å for **1** and 2.1035(13) and 2.0901(13) Å for **2**, the shorter distance being on the methyl side of maltolate. The coordinated maltolate ligand is almost planar with torsion angles (M-O-C-C) of 173–179°. No intermolecular arene ring stacking is observed, but several directional hydrogen bonds ($\measuredangle$D–H···A $150 < \theta < 180°$) are present between independent molecules in the crystal structures of both **1** and **2**·2H$_2$O. Three different types of interactions link together four independent molecules of [Os(η⁶-*p*-cym)(mal)Cl] (**1**). One set of dimers is formed in the crystal structure through four short-range interactions between an oxygen atom of the coordinated maltolate and *p*-cymene protons of a second molecule, O21(mal)···H71(*p*-cym) 2.57 Å and O21(mal)···H102(isopropyl *p*-cym) 2.67 Å. Another set of dimers is formed between the chloride (Cl1) and a *p*-cym ring proton (H41) of another molecule (2.56 Å). Finally, short-range interactions are present between C24–H171 of the maltolate backbone and both a chloride (Cl1 2.77 Å) and a maltolate oxygen (O21 2.36 Å) of an adjacent molecule (Figure S2 and Table 4).

Similar short-range interactions are also present in crystals of the Ru analogue, which crystallised with two solvent molecules of water (**2**·2H$_2$O). The latter forms similar dimers to those found in crystals of **1**, involving the interactions O12(mal)···H10A(isopropyl *p*-cym) (2.67 Å) and the chloride (Cl1) of one molecule and a *p*-cymene ring proton (H61) of another (2.90 Å). An H-bond (2.37 Å) forms between C52 and H52 of the maltolate backbone and maltolate O12 of an adjacent molecule (Figure S3). The hydrogen atoms of the two solvent water molecules were located (in a difference map, but placed in ideal positions and not refined) and form a chain, which is flanked by the Ru complex on either side (Figure 4a). The solvent molecules form a ring of H-bonds involving H4W···Cl1 (2.52 Å; O2W···Cl1 3.240(2) Å) and H1W···O22(mal) (2.09 Å), with water molecules separated by 2.852(3) Å (O1W–O2W; Figure 4b and Table 4).

NMR studies of chemical exchange: In the ^{1}H NMR spectra of the maltolato complexes **1** and **2** in CDCl$_3$ there were doublets for each of the four *p*-cymene ring protons (integrating to 1H each) and two doublets for the *p*-cymene isopropyl methyl groups (Figures 5a and S4). However, in the ^{1}H NMR spectra of **1** and **2** in D$_2$O, mainly present as the aqua adducts **1a** and **2a** (see below), there were only two doublets for the coordinated ring protons (integrating to 2H each) and one doublet (integrating as 6H) for the two CH$_3$ groups belonging to the isopropyl group (Figures 5c and S4). Chemical shifts for the aqua complex are pH sensitive, see Figure S6. The spectra of **1** in another non-coordinating

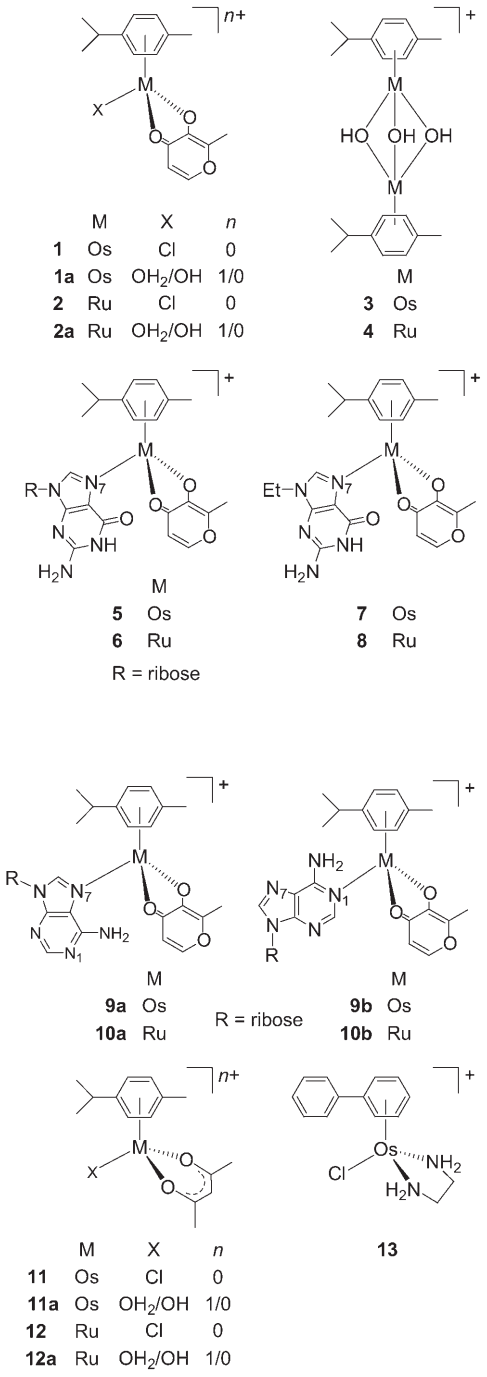

	M	X	*n*
1	Os	Cl	0
1a	Os	OH_2/OH	1/0
2	Ru	Cl	0
2a	Ru	OH_2/OH	1/0

	M
3	Os
4	Ru

	M
5	Os
6	Ru

	M
7	Os
8	Ru

R = ribose

	M
9a	Os
10a	Ru

	M
9b	Os
10b	Ru

	M	X	*n*
11	Os	Cl	0
11a	Os	OH_2/OH	1/0
12	Ru	Cl	0
12a	Ru	OH_2/OH	1/0

13

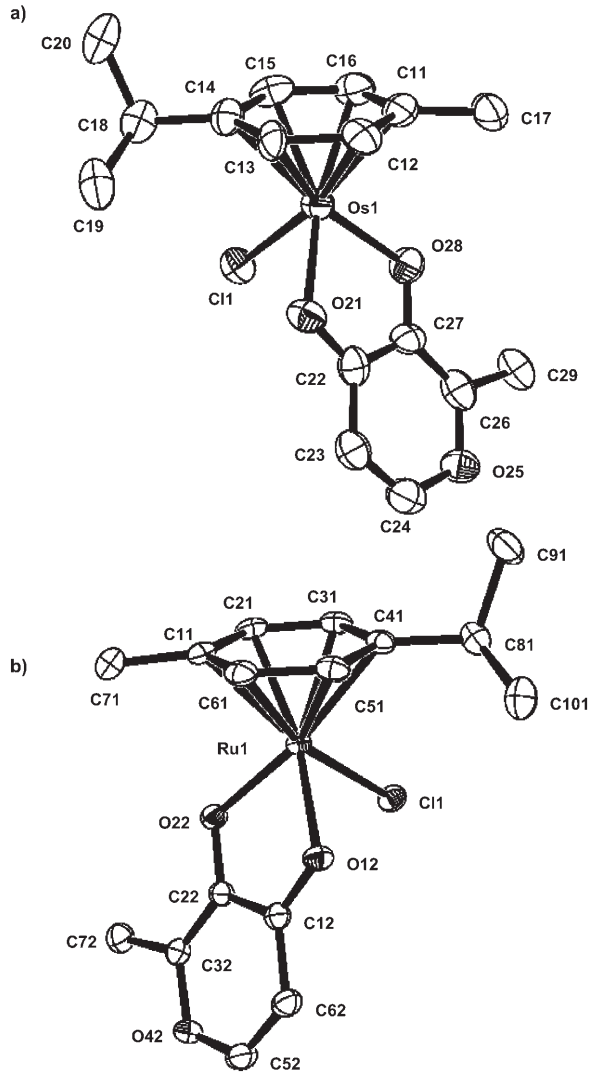

Figure 3. ORTEP diagrams and atom numbering scheme for a) [Os(η^6-*p*-cym)(mal)Cl] (**1**) and b) [Ru(η^6-*p*-cym)(mal)Cl] (**2**) (50 % probability ellipsoids). The hydrogen atoms have been omitted for clarity.

solvent, deuterated toluene, consisted of two overlapped doublets and two doublets for the *p*-cymene ring protons, as well as two overlapped doublets for the *p*-cymene isopropyl group (Figure 5b). However, in deuterated methanol the spectrum of **1** (Figure 5d) shows broad peaks for the aromatic protons, again with only two peaks for the *p*-cymene ring protons and a single doublet for the two isopropyl CH_3 groups. The two broad peaks for the *p*-cymene ring protons ($\delta = 6.16$ and 5.92 ppm) sharpened to doublets at higher temperatures (323 K) and split into two doublets ($\delta = 6.20$ and 6.17 ppm) and a doublet of doublets ($\delta = 5.92$ ppm) at lower temperatures (223 K; see Figures 6 and S5). At the coalescence temperature ($T_c = 283$ K), the rate of the dynamic process was determined to be $k_c = 25.9\ s^{-1}$, with lifetimes of the separate isomers of $t_c = 40$ ms and an activation energy $E_a = 61.5\ kJ\,mol^{-1}$ at T_c.

Hydrolysis and acidity of aqua adducts: Complexes **1** and **2** hydrolysed rapidly in aqueous solution to give predominantly the monoaqua complexes [Os(η^6-*p*-cym)(mal)(OH_2)]$^+$ (**1a**) and [Ru(η^6-*p*-cym)(mal)(OH_2)]$^+$ (**2a**), respectively. The pK_a values of the coordinated water in **1a** and **2a** were found to be 7.60 ± 0.02 and 9.23 ± 0.02, respectively (Figure S6). A second hydrolysis product, the hydroxo-bridged dimer [(η^6-*p*-cym)M(μ-$OH)_3$M(η^6-*p*-cym)]$^+$ M = Os (**3**) and Ru (**4**), also formed (though less readily for Ru) and increased in concentration with increase in pH. More detailed

Table 2. Crystallographic data for [Os(η^6-*p*-cym)(mal)Cl] (**1**) and [Ru(η^6-*p*-cym)(mal)Cl]·2 H_2O (**2**·2 H_2O).

	1	**2**·2 H_2O
formula	$C_{16}H_{19}ClO_3Os$	$C_{16}H_{23}ClO_5Ru$
M_w	484.98	431.86
crystal description	brown tablet	red lath
crystal size [mm]	0.37×0.24×0.11	0.96×0.30×0.17
λ [Å]	0.71073	0.71073
T [K]	150	150
crystal system	monoclinic	monoclinic
space group	$P2_1/c$	$P2_1/c$
a [Å]	11.8586(6)	13.6816(4)
b [Å]	9.1697(5)	8.9244(2)
c [Å]	15.4833(8)	14.46911(4)
α [°]	90	90
β [°]	109.535(4)	96.783(2)
γ [°]	90	90
V [Å^3]	1586.74(15)	1754.31(8)
Z	4	4
R	0.0566	0.0275
R_w	0.0915	0.0620
goodness-of-fit	0.6705	1.079

Table 3. Selected bond lengths [Å] and angles [°] for [Os(η^6-*p*-cym)(mal)Cl] (**1**) and [Ru(η^6-*p*-cym)(mal)Cl]·2 H_2O (**2**·2 H_2O).

Bond(s)[a]	**1**	**2**·2 H_2O
	Length/angle	
M–C (arene)	2.181(7)	2.1887(19)
	2.172(6)	2.1543(19)
	2.136(6)	2.1593(19)
	2.190(7)	2.1880(18)
	2.178(7)	2.1445(18)
	2.162(7)	2.1717(19)
M–Cl	2.4326(16)	2.4329(5)
M–O1	2.114(4)	2.1035(13)
M–O2	2.091(5)	2.0901(13)
O1-M-O2	78.67(18)	78.79(5)
O1-M-Cl	81.88(13)	83.42(4)
Cl-M-O2	84.92(13)	85.89(4)

[a] M = Os^{II} or Ru^{II}; O1 carbonyl side of maltolate, O2 methyl side of maltolate (see Figure 3).

Table 4. Selected hydrogen-bond lengths [Å] and angles [°] for complexes **1** and **2**·2 H_2O.

[Os(η^6-*p*-cym)(mal)Cl] (**1**)			
D–H···A	*d*(H···A)	*d*(D···A)	∢DHA
C13–H71···O21 (inter)	2.57	3.555(8)	167
C19–H102···O21 (inter)	2.67	3.619(9)	158
C16–H41···Cl1 (inter)	2.56	3.554(7)	170
C24–H171···O21 (inter)	2.36	3.281(8)	153
C24–H171···Cl1 (inter)	2.77	3.511(7)	132
[Ru(η^6-*p*-cym)(mal)Cl]·2 H_2O (**2**·2 H_2O)			
D–H···A	*d*(H···A)	*d*(D···A)	∢DHA
C101–H10A···O12 (inter)	2.67	3.449(3)	136
C61–H61···Cl1 (inter)	2.90	3.7625(19)	152
C52–H52···O12 (inter)	2.37	3.288(2)	163
O2W–H4W···Cl1 (inter)	2.52	3.240(2)	169
O1W–H1W···O22 (inter)	2.09	2.805(2)	174
O1W–H2W···O2W (inter)	2.04	2.852(3)	164
O2W–H3W···O1W (inter)	2.03	2.771(3)	180

results of the hydrolysis studies and pH titrations can be found in the Supporting Information.

Aqueous stability of complexes 1 and 2; speciation under biological test conditions: Solutions of **1** were prepared so as to mimic those being used in the cytotoxicity tests. ^{1}H NMR spectra (800 MHz) of solutions of **1** at concentrations of 2 and 50 μM in 0.125% [D_6]DMSO/99.875% D_2O, at physiological pH (approximately 7.3), were recorded directly after sample preparation (≈10 min, 298 K) and after incubation at 310 K for 24 h. ^{1}H NMR peaks (δ = 6.04 and 5.82 ppm) for the hydroxo-bridged dimer [(η^6-*p*-cym)Os(μ-OH)$_3$Os(η^6-*p*-cym)]$^+$ (**3**) predominate under these conditions, as determined by ^{1}H NMR and electrospray ionisation mass spectrometry (ESIMS, Figure S7; 100% **3** at 2 μM after 10 min and after 24 h at 310 K, and at 50 μM approximately 28% **3** after 10 min and approximately 65% after 24 h at 310 K). Solutions prepared in the absence of [D_6]DMSO gave similar results. Solutions (8 and 200 μM) were also prepared in the presence of 100 mM NaCl and the ^{1}H NMR spectra were recorded as previously. Based on peak integrals, the hydroxo-bridged dimer **3** predominates at 8 μM **1** after incubation at 310 K for 24 h, whereas at 200 μM **1** approximately 24% **3** was present after 10 min at 298 K and approximately 61% **3** after 24 h at 310 K.

Solutions of the maltolato complexes **1** and **2**, as well as of the acac complexes **11** and **12**, were prepared at varying concentrations (2 and 1 mM, 500, 250, 100, 50 and 20 μM) in D_2O, and incubated at 310 K for 24 h before recording their ^{1}H NMR spectra at 298 K. Peaks corresponding to the *p*-cymene ring protons of the aqua complex, [M(η^6-*p*-cym)(XY)(OD_2/OD)]$^{+/0}$ (M = Os, XY = mal, **1a**; M = Ru, XY = mal, **2a**; M = Os, XY = acac, **11a**; M = Ru, XY = acac, **12a**), dominated the ^{1}H NMR spectra of the more concentrated solutions. As the concentrations of complexes were decreased, the peaks corresponding to species **3** (δ = 6.04 and 5.82 ppm) and **4** (δ = 5.37 and 5.17 ppm) increased in intensity, as did those for the free maltol and acacH ligands, whereas those for the aqua complexes (**1a**, **2a**, **11a** and **12a**) decreased in intensity (Figures 7 and S8). Based on ^{1}H NMR peak integrals for the *p*-cymene ring protons, the aqua complex **1a** accounted for 71% of the initial Os–maltolato complex **1** at 2 mM; however, at 20 μM this was much lower at 30%. A higher proportion of the Ru–aqua complex **2a** was present for **2** (85% at 2 mM and 38% at 20 μM; Figure 7). Only 61% of the Os–aqua–acac complex **11a** was present at 2 mM **11** and this decreased to 0% at 100 μM **11**. More of the Ru–aqua–acac complex **12a** (79%) was present for 2 mM solutions of **12**, but this also decreased to 0% at 20 μM **12** (Figure S8). ESIMS of equilibrium NMR spectroscopic samples of **2** and **12** at 50 μM (containing predominantly peaks for hydroxo-bridged dimer **4**) gave peaks at *m*/*z*: 525.1 and 526.1, respectively, assignable to [(η^6-*p*-cym)Ru(μ-OD)$_3$Ru(η^6-*p*-cym)]$^+$ (**4**; calcd *m*/*z*: 526.1). The proportion of the metal present as the hydroxo-bridged dimer **3** (Os) or **4** (Ru) is plotted against initial complex concentration in Figure 8.

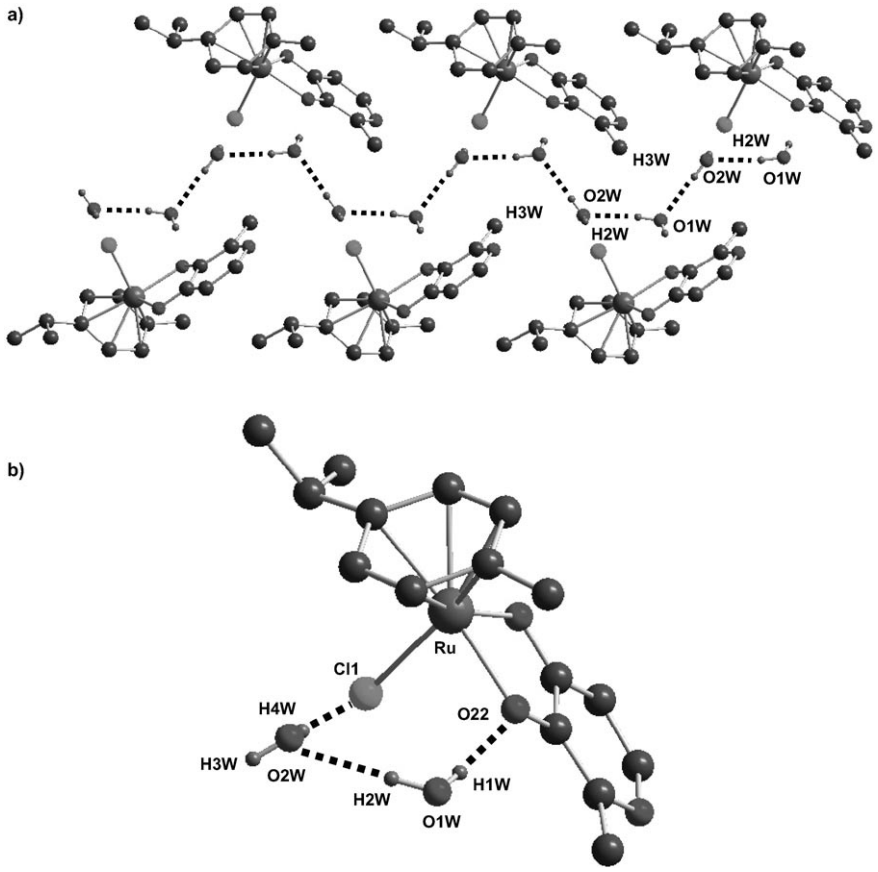

Figure 4. X-ray crystal structure of **2**·2H_2O showing a) the chain of water molecules flanked by ruthenium complexes and b) the ring of H-bonds formed between the water molecules and the complex; H4W···Cl1 (2.52 Å) and H1W···O22(mal) (2.09 Å). Pictures prepared by using the program Diamond.

Interactions with nucleobases: The monoaqua complexes **1a** and **2a** react rapidly with N7 of G (guanosine and 9-ethylguanine) and both N7 and N1 of A (adenosine) nucleobases. Assigned NMR spectra (including selected pH titrations) for these reactions can be found in the Supporting Information (Figures S9–S14).

The addition of 1 mol equiv cytidine (Cyt) or thymidine (Thy) to an equilibrium solution of **1** (in D_2O at 298 K, pH* 7.01 and 6.67) resulted in no additional peaks in the ^{1}H NMR spectrum, even after incubation at 310 K for 20 h (Figure S14).

Stability of 9-ethylguanine adducts: Solutions of the 9-EtG adduct $[Os(\eta^6\text{-}p\text{-cym})(mal)(9EtG)]^+$ (**7**) in D_2O at varying concentrations (20 μM–2 mM) were prepared and their ^{1}H NMR spectra recorded within 10 min of sample preparation at 298 K (Figure 9), as well as after incubation at 310 K for 24 h (Figure S15). At high concentrations, peaks for **7** dominated (77% **7** at 2 mM), but as the complex concentration decreased, peaks for the aqua complex **1a**, free maltol and hydroxo-bridged dimer **3** increased in intensity (29% **7** at 20 μM). At approximately 200 μM **7**, 50% of the 9-EtG remained bound. The apparent formation constant for **7** was determined as $\log K = 4.32 \pm 0.02$ from the species distribution plot in Figure 10. After incubation at 310 K for 24 h, complex **7** still dominated at high concentration (69% **7** at 2 mM), but free maltol and the hydroxo-bridged dimer **3** dominated at lower concentrations (0% **7** at 20 μM; Figure S15).

The 9-EtG complex **7** and the Ru analogue **8** were also prepared in situ at varying concentrations by mixing equimolar solutions of **1** or **2** and 9-EtG so that the final concentrations were 20 μM–1 mM. ^{1}H NMR spectra were recorded after approximately 10 min at 298 K, as well as after incubation at 310 K for 24 h (Figure S16). For reactions of the Os–maltolato complex **1** with 9-EtG, 73% of 9-EtG-bound adduct **7** was formed at 1 mM and only 31% at 20 μM; for the Ru analogue, 64% of the 9-EtG-bound adduct **8** formed at 1 mM, but none at 20 μM and little further change occurred over 24 h (310 K). Values for the formation constants were determined as $\log K = 4.41 \pm 0.04$ for the Os complex **7** and 3.87 ± 0.09 for the Ru complex **8** (Figure S17).

Cytotoxicity: Complexes **1** and **2** were non-toxic towards the human lung A549 and ovarian A2780 cancer cell lines at concentrations up to 50 μM (the highest test concentration). The IC_{50} values are therefore likely to be >100 μM and the complexes are deemed inactive.[27]

Discussion

Mechanism of hydrolysis: Density functional theory (DFT) calculations support the experimental observation of faster hydrolysis of Os^{II}–arene complexes containing anionic O,O-chelating ligands compared to analogous complexes with the neutral N,N-chelating diamine ligand en. The barrier for hydrolysis of $[Os(\eta^6\text{-}p\text{-cym})(acac)Cl]$ (**11**) is significantly lower (by nearly 30 kJ mol^{-1}) than that for the en complex $[Os(\eta^6\text{-biphenyl})(en)Cl]^+$ (**13**). A simple rationalisation is that it is harder to remove Cl^- from the monocationic $[Os(\eta^6\text{-arene})(en)Cl]^+$ species than from the neutral $[Os(\eta^6\text{-arene})(acac)Cl]$.

Interestingly, the incoming water molecule forms H-bonds to the oxygen of the coordinated acac ligand (Figure 2).

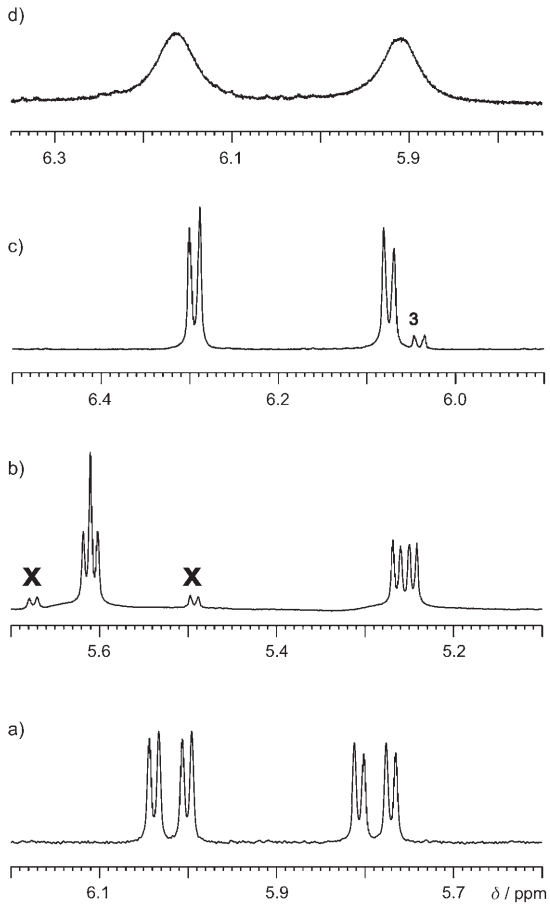

Figure 5. Low-field region of the ^{1}H NMR spectrum (298 K) of **1** (containing resonances for the *p*-cymene ring protons) in the non-coordinating solvents a) $CDCl_3$ (doublets at $\delta = 6.04$, 6.00, 5.81 and 5.77 ppm) and b) [D_8]toluene (two overlapped doublets $\delta = 5.61$ ppm and two doublets $\delta = 5.26$ and 5.25 ppm) (x = unidentified species accounting for $\approx 15\%$ of Os), and in the coordinating solvents c) D_2O (two doublets, peak position pH sensitive and a doublet at $\delta = 6.04$ ppm for **3**) and d) [D_4]MeOD (two broad peaks at $\delta = 6.16$ and 5.92 ppm).

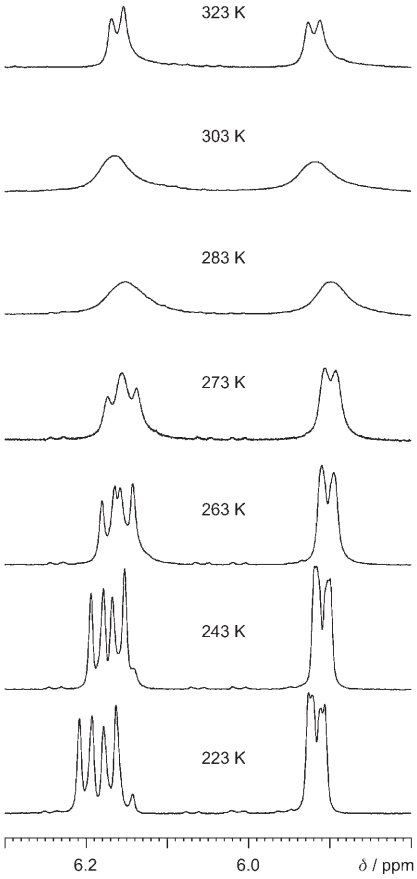

Figure 6. Low-field region of the ^{1}H NMR spectrum of **1** in [D_4]MeOD at varying temperatures. The four non-equivalent *p*-cymene ring protons resolve into two doublets ($\delta = 6.20$ and 6.17 ppm) and two closely overlapping doublets ($\delta = 5.92$ ppm) at 223 K, broaden ($\delta = 6.16$ and 5.92 ppm) at 283 K (coalescence temperature, T_c) and sharpen into two doublets at 323 K ($\delta = 6.16$ and 5.92 ppm).

However, this orientation in the transition state does mean that the water must reorganise itself to form the final product. The calculated activation energy for hydrolysis of the Os^{II}–en complex **13** is slightly larger than that of the Ru^{II} analogue reported previously (by ≈ 20 kJ mol^{-1}),[28] which appears to explain the observed slower rate of hydrolysis of the Os^{II}–en complex compared to its Ru^{II} analogue.[10]

Structures of maltolato complexes: There appear to be no previous reports of structures of maltolato complexes of Os^{II} arenes, although that of a Ru^{II} complex [Ru(η^6-mes)(mal)Cl] has been reported.[22] The structures of the Os (**1**) and Ru (**2**·2H_2O)–maltolato complexes are very similar. In the context of hydrolysis (which is rapid for both **1** and **2**), it is interesting to note that they have the same metal–chloride bond lengths of 2.43 Å, which are significantly longer than those for the N,N-chelated complexes [M(η^6-biphenyl)(en)Cl]$^+$ (2.3963(14) Å M = Os, 2.4005(10) Å M = Ru).[10] The metal–oxygen bond lengths in **1** and **2**·2H_2O (2.09–2.11 Å) are longer than those in their respective acac analogues (2.0700(16)–2.078(3) Å).[10,11] Both the M–O bond lengths for the Os complex **1** are greater than those for the Ru complex **2**·2H_2O, with the longer M–O bonds being on the carbonyl side of the maltolate ligand. The Ru–O (2.106(4) and 2.091(4) Å) and Ru–Cl (2.420(2) Å) bond lengths[22] in [Ru(η^6-mes)(mal)Cl] are similar to those of **2**·2H_2O.

In the X-ray structure of the hydrated Ru^{II} complex **2**·2H_2O (Figure 4b), two water molecules are involved in H-bonding to bound chloride and one of the bound malolate oxygen atoms. This arrangement is similar to that found in the calculated transition state for aquation of the related Os^{II}–acac complex **11** (Figure 2a), in which a hydrogen (H1W) from one of the water molecules forms a hydrogen bond with a maltolate oxygen (O22 in **2**·2H_2O), and hence the solid-state structure appears to provide a "snapshot" of the possible hydrolysis pathway. The O2W···Cl distance of 3.240(2) Å compares well with the values reported for the similarly hydrated Ru^{II}–picolinate complex [Ru(η^6-mes)-

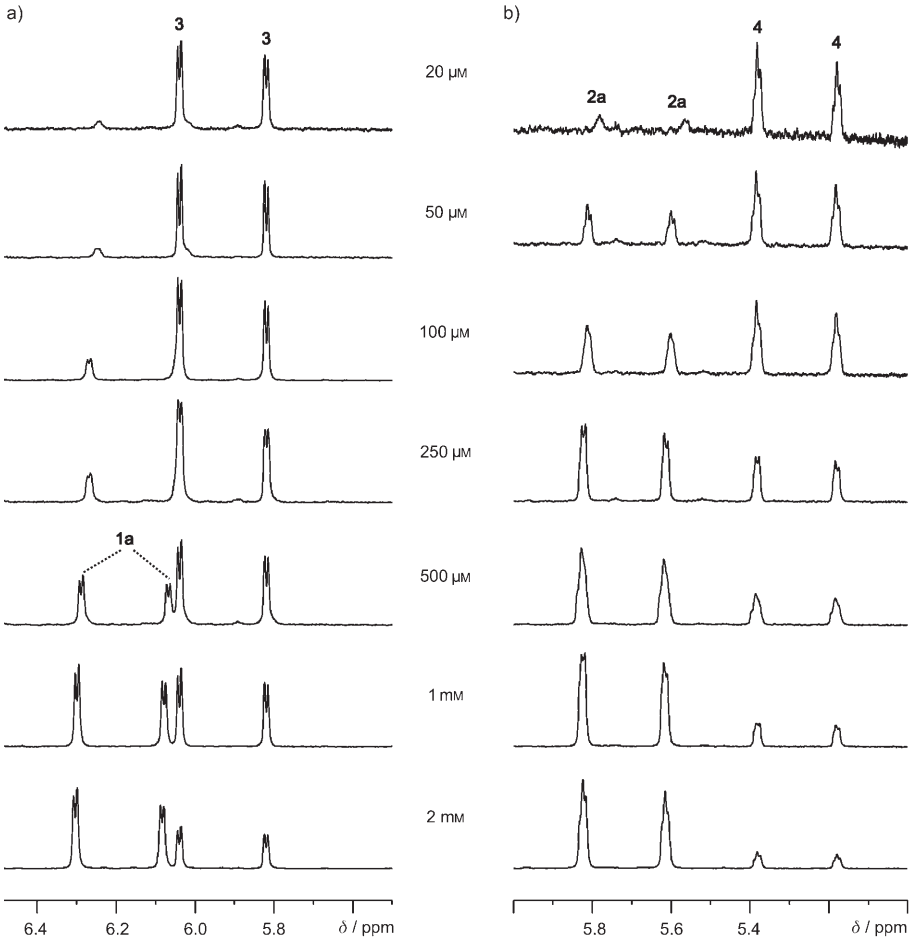

Figure 7. Low-field region of the ^{1}H NMR spectra (298 K) of complexes **1** (a) and **2** (b) at concentrations varying from 2 mM to 20 μM after incubation at 310 K for 24 h. **1a** and **2a** correspond to the aqua complexes $[Os(\eta^6\text{-}p\text{-cym})(mal)(OD_2)]^+$ and $[Ru(\eta^6\text{-}p\text{-cym})(mal)(OD_2)]^+$, respectively, and **3** and **4** to the hydroxo-bridged dimers $[(\eta^6\text{-}p\text{-cym})Os(\mu^3\text{-OD})_3Os(\eta^6\text{-}p\text{-cym})]^+$ and $[(\eta^6\text{-}p\text{-cym})Ru(\mu^3\text{-OD})_3Ru(\eta^6\text{-}p\text{-cym})]^+$, respectively.

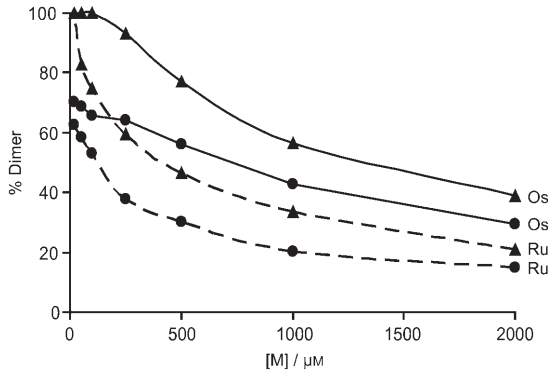

Figure 8. Dependence of formation of the hydroxo-bridged dimer (based on NMR peak integrals) on total metal concentration for solutions of the osmium and ruthenium–maltolato (**1** and **2**) and acac complexes (**11** and **12**), $[M(\eta^6\text{-}p\text{-cym})(XY)Cl]$, in D_2O after incubation at 310 K for 24 h. ----- M = Ru, —— M = Os, ● XY = mal, ▲ XY = acac. The most stable complex towards dimer formation is the ruthenium–maltolato complex $[Ru(\eta^6\text{-}p\text{-cym})(mal)Cl]$ (**2**), and the least stable is the osmium acac complex $[Os(\eta^6\text{-}p\text{-cym})(acac)Cl]$ (**11**).

$(NC_5H_4CO_2)Cl]\cdot 3H_2O$ (3.24 Å).[21] In both cases, two water molecules form a ring of hydrogen-bonding interactions (Cl·(H)·O·(H)·O·(H)·X) and appear to be preorganised for hydrolysis.

Dynamic O,O-chelate ring opening: The presence of a chiral Os centre in complex **1**, due to the unsymmetrical nature of maltolate, is evident in ^{1}H NMR spectra in non-coordinating solvents ($CDCl_3$ and $[D_8]$toluene), the four *p*-cymene ring protons and two isopropyl methyl groups being non-equivalent. In coordinating proton-donor solvents, such as D_2O and $[D_4]$MeOD, a dynamic process appears to take place at the metal centre on a millisecond timescale even at 283 K. This probably involves either ring opening of coordinated maltolate aided by the coordinating proton-donor solvent, flipping and rebinding, or inversion at the Os centre by a mechanism similar to that proposed by Davies et al.[29] This dynamic process is faster in D_2O than in $[D_4]$MeOD, and such a dynamic process may contribute to the mechanism of maltolate displacement in water.

Hydrolysis: The hydrolysis of complexes **1** and **2** is rapid in water, with one major set of ^{1}H NMR peaks present (corresponding predominantly to the aqua complex). Such rapid hydrolysis in comparison to the N,N-chelated en complexes probably results from the increased electron density at the metal centre due to the anionic maltolate ligand, as well as possible stabilising interactions between hydrogen atoms of coordinated water and the oxygen atoms of the chelated ligand. The rapid hydrolysis of complexes **1** and **2**, and the proposed stabilising H-bonds between the maltolate oxygen atoms and the hydrogen atoms of incoming water molecules, are in accordance with the DFT calculations for the hydrolysis of the similar complex **11** containing the anionic O,O-chelating acac ligand. The Os^{II} complex **13** hydrolyses about 40 times more slowly than the Ru^{II} analogue at physiological pH,[10] but the hydrolysis rates for the Os^{II} and Ru^{II}–maltolato complexes were both too fast to measure (by NMR spectroscopy).

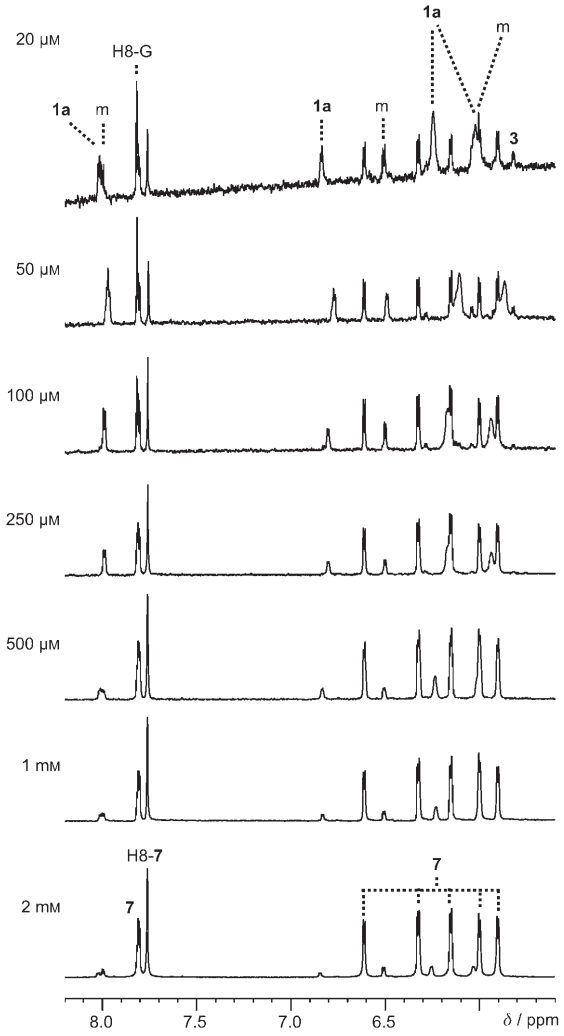

Figure 9. Low-field region of the ^{1}H NMR spectrum (298 K) of [Os(η^6-*p*-cym)(mal)(9EtG)]$^+$ (**7**) at varying concentrations (2 mM to 20 μM), recorded directly after sample preparation. **1a** is the aqua complex [Os(η^6-*p*-cym)(mal)(OD$_2$)]$^+$, H8-G the H8 peak for unbound 9-ethylguanine, **3** the hydroxo-bridged dimer and m free maltol.

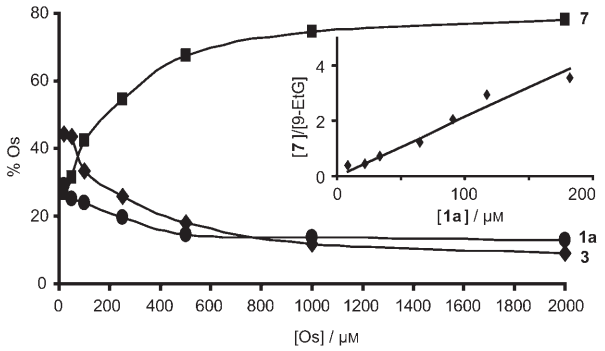

Figure 10. Plot showing the distribution of {Os(η^6-*p*-cym)}$^{2+}$ amongst the species **7** [Os(η^6-*p*-cym)(mal)(9EtG)]$^+$ (■), the aqua complex **1a** (●) and the hydroxo-bridged dimer **3** (♦). The inset shows a plot of [**7**]/[free 9-EtG] versus [**1a**], based on integration of ^{1}H NMR peaks (Figure 9). An equilibrium constant of $\log K = 4.32 \pm 0.02$ was calculated from the slope.

Acidity of aqua complexes: The pK_a values for the Os–maltolato–aqua complex **1a** (7.60) and Ru analogue (9.23) are approximately 1 pK_a unit higher in comparison to those of complexes containing the neutral en ligand,[10,30] but in a similar range to those of the corresponding acac complexes, Table S1.[10,11] Water is significantly more acidic (by $\approx$1.6 pK_a units) when coordinated to Os^{II} compared to Ru^{II}, as has been reported for some other complexes.[8,10] The implications of these pK_a values are that at physiological pH (7.4) a significant portion (approximately 40%) of complex **1a** would be present as the less reactive hydroxo species [Os(η^6-*p*-cym)(mal)(OH)], whereas almost all (>95%) of complex **2a** would be present as the reactive aqua complex [Ru(η^6-*p*-cym)(mal)(OH$_2$)]$^+$.

The lower pK_a value (that is, higher affinity for hydroxide) of the Os–aqua complex **1a** could contribute to the finding that the Os–maltolato complex **1** forms the hydroxo-bridged dimer more readily and at lower pH values than its Ru analogue **2**. It seems likely that one of the maltolate oxygen atoms (probably the deprotonated oxygen adjacent to the methyl group) accepts a proton from the suitably positioned coordinated water, and does so more readily from the more acidic water coordinated to Os compared to Ru, leading to chelate ring opening and eventual loss of maltol and formation of the stable hydroxo-bridged dimer **3**.

Stability of complexes under biological test conditions: Our work shows that the introduction of the five-membered maltolate chelate ring provides significant stabilisation towards hydroxo-bridged dimer formation in comparison to the six-membered acac complexes,[10] but the dominant species present in aqueous solution under conditions relevant to the biological tests (micromolar concentrations, pH$\approx$7, 24 h exposure at 310 K) for both the Os^{II}–maltolato complex **1** and Ru^{II} analogue **2** are the hydroxo-bridged dimers **3** and **4**, respectively (Figure 8). Remarkably, even in solutions of **1** (8 and 200 μM) containing 0.1 M NaCl, the hydroxo-bridged dimer was the major species present, implying that the high levels of chloride in blood plasma would not prevent hydroxo-bridged dimer formation and deactivation of the complexes.

Hydroxo-bridged dimers form most readily from [Os(η^6-*p*-cym)(acac)Cl] (**11**), and least readily from [Ru(η^6-*p*-cym)-(mal)Cl] (**2**; Figure 8). The higher acidity of water coordinated to Os^{II} compared to Ru^{II} (approximately 1.6 pK_a units) probably contributes to the easier protonation of O,O-chelated ligands in Os complexes. Both maltolate and acetylacetonate are readily protonated at physiological pH values, the conjugate acids of the free ligands produce pK_a values of 8.62 and 8.88, respectively.[31] A possible mechanism for the formation of the hydroxo-bridged dimers **3** and **4** involves protonation of one of the maltolate oxygen atoms followed by ring opening and eventual loss of the maltolate, although the intermediates, if they are formed, must be short-lived as they were not detected in our experiments. It is interesting to note that coordinated water in the triaqua benzene complex [Os(η^6-benzene)(OH$_2$)$_3$]$^{2+}$ is thought to be

highly acidic ($pK_a \approx 2.3$–3.4).[7] Thus, on loss of coordinated maltolate, deprotonation of other coordinated aqua ligands is likely to occur readily.

Interactions with nucleobases: DNA is an important potential biological target for many metal-based anticancer agents.[32] Distortions of DNA structure often correlate with anticancer activity.[33] Little work has been reported on the reactivity of Os complexes towards DNA nucleobases.

Both Os^{II} and Ru^{II}–maltolato complexes **1** and **2** reacted similarly with nucleobases. Binding was rapid (< 10 min, by the time the first ^1H NMR spectrum was recorded) and selective for purine bases (Guo, 9-EtG and Ado). There was no reaction with the pyrimidine bases (Cyt or Thy). This observation of similar reactivity of both Os^{II} and Ru^{II} is notable in view of the inertness often associated with third-row transition metals (Os) compared to their lighter congeners (Ru).

Despite the reactivity of the Os–maltolato complex **1** towards DNA nucleobases, it was found to be non-toxic towards both the human lung A549 and ovarian A2780 cancer cell lines at concentrations up to 50 μM (the highest test concentration). The Ru analogue **2** is also inactive, although the acac analogue of **2** is cytotoxic ($IC_{50} = 19$ μM towards A2780 cells).[4]

The species $\{Os(\eta^6\text{-}p\text{-cym})(mal)\}^+$ appears to bind more strongly to 9-EtG ($\log K \approx 4.4$) compared to the Ru analogue ($\log K \approx 3.9$). These appear to be the first determinations of stability constants for metal–arene–nucleobase adducts, although binding constants for DNA-intercalating Ru^{II}–arene complexes have been reported.[34] However, as the binding is relatively weak, high concentrations of the complex might need to reach DNA in the nucleus for effective lesions (and cytotoxicity) to occur. Unlike DNA platination,[35] binding of complexes **1** and **2** to DNA nucleobases is likely to be reversible and the lesions more readily repaired by enzymes. The formation of hydroxo-bridged dimers (**3** and **4**) provides a driving force for the dissociation of nucleobase adducts. These dimers appear to be the thermodynamically stable products from the dissociation of nucleobase adducts in aqueous solution (Figures S15 and S16 and Scheme 1).

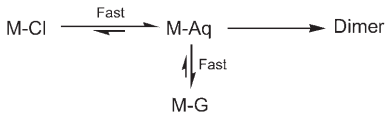

Scheme 1. General scheme for hydrolysis and nucleobase binding to complexes **1** and **2**. Hydrolysis is rapid, as is binding to the G nucleobase. However, with time the hydroxo-bridged dimer predominates as the thermodynamically more stable product.

Conclusion

Chloro–Os^{II}–arene complexes containing the anionic O,O-chelating maltolate ligand are highly reactive in aqueous solution. They hydrolyse and bind to purine nucleobases rapidly, properties shared by Ru^{II}–acac analogues which are cytotoxic to cancer cells.[4] The rapid hydrolysis of these O,O-chelated complexes compared to the N,N-chelated en complex is supported by DFT calculations, which suggest that the former reactions are appreciably more dissociative than the latter; chloride is harder to remove from the monocationic en species compared to the neutral acac or mal species. Interestingly, the ordering of water molecules around the chloro complex in the calculated transition state for the hydrolysis of $[Os(\eta^6\text{-}p\text{-cym})(acac)Cl]$ resembles that observed in the X-ray crystal structure of the hydrated Ru–maltolato complex **2**·2 H_2O. However, reorganisation of water is necessary for formation of the final aqua product.

The presence of a five-membered maltolate chelate ring increases the hydrolytic stability of these metal–arene complexes compared to the acac analogues. However, they are still deactivated to a significant extent at biologically relevant (micromolar) concentrations by formation of inert hydroxo-bridged dimers, even in the presence of 100 mM NaCl. These findings highlight the importance of probing the aqueous chemistry at low micromolar concentrations when complexes are designed for biological applications.

The evidence for facile maltolate ring opening on a millisecond timescale, even at 283 K (Figure 6), and the lower pK_a value of water coordinated to $\{Os(\eta^6\text{-}p\text{-cym})(mal)\}^+$ (7.60) compared to that of Ru (9.23), suggests that the mechanism of dimer formation involves protonation of bound maltolate by coordinated water, ring opening and loss of coordinated maltolate. The higher acidity of coordinated water may favour protonation of maltolate on Os^{II} compared to Ru^{II}, and the higher affinity for hydroxide may lead to direct substitution of maltolate in basic solutions.

The binding of purine nucleobases to $\{Os/Ru(\eta^6\text{-}p\text{-cym})(mal)\}^+$ is rapid and reversible, the dissociation of the adducts being driven by the high thermodynamic stability of the hydroxo-bridged dimers, especially for Os. Intriguingly, binding of $\{Os(\eta^6\text{-}p\text{-cym})(mal)\}^+$ to 9-EtG appears to be stronger than that for the Ru^{II} analogue. However, the binding of both these Os and Ru complexes to G nucleobases is relatively weak and labile, which may not only allow efficient removal and repair of DNA adducts in cells, but also give rise to the formation of stable hydroxo-bridged dimers.

Experimental Section

Materials: Sodium methoxide and 3-hydroxy-2-methyl-4-pyrone were purchased from Sigma-Aldrich, deuterated solvents from Aldrich, and $OsCl_3 \cdot nH_2O$ and $RuCl_3 \cdot nH_2O$ from Alfa Aesar. $[Os(\eta^6\text{-}p\text{-cym})Cl_2]_2$, $[Ru(\eta^6\text{-}p\text{-cym})Cl_2]_2$, $[Os(\eta^6\text{-}p\text{-cym})(acac)Cl]$ and $[Ru(\eta^6\text{-}p\text{-cym})(acac)Cl]$ were prepared by previously reported procedures.[10,11,36–38]

$[Os(\eta^6\text{-}p\text{-cym})(mal)Cl]$ (1): A solution of maltol (41.7 mg, 0.33 mmol) and sodium methoxide (17.7 mg, 0.33 mmol) in MeOH (5 mL) was stirred at ambient temperature for 45 min and added to a solution of $[Os(\eta^6\text{-}p\text{-cym})Cl_2]_2$ (99.2 mg, 0.125 mmol) in MeOH (5 mL) under argon. The resulting mixture was stirred at ambient temperature under argon for 3 h, the solvent removed on a rotary evaporator, and the residue extracted with dichloromethane followed by filtration through a glass-wool plug. The solvent was again removed on a rotary evaporator and the product

was redissolved in the minimum amount of acetone. Diethyl ether was added and after storage at 253 K overnight, the yellow product was recovered by filtration. It was washed with diethyl ether (10 mL) and air-dried. Yield: 105.6 mg (87%); ^{1}H NMR ($CDCl_3$): δ = 7.57 (d, J = 5.0 Hz, 1H), 6.59 (d, J = 5.0 Hz, 1H), 6.04 (d, J = 5.3 Hz, 1H), 6.00 (d, J = 5.3 Hz, 1H), 5.81 (d, J = 5.3 Hz, 1H), 5.77 (d, J = 5.5 Hz, 1H), 2.74 (sept, J = 6.9 Hz, 1H), 2.44 (s, 3H), 2.35 (s, 3H), 1.30 (d, J = 6.9 Hz, 3H), 1.27 ppm (d, J = 7.1 Hz, 3H); elemental analysis calcd (%) for $C_{16}H_{19}ClO_3Os$ (485.00): C 39.62, H 3.95; found: C 39.70, H 3.78. Crystals suitable for X-ray diffraction were obtained by slow evaporation from a dichloromethane/diethyl ether solution at 253 K.

[Ru(η^6-*p*-cym)(mal)Cl] (2): [Ru(η^6-*p*-cym)(Cl)$_2$]$_2$ (203.7 mg, 0.33 mmol) was stirred in MeOH (15 mL) at ambient temperature for 1 h. Maltol (109.1 mg, 0.87 mmol) and sodium methoxide (49.0 mg, 0.91 mmol), which had been stirred in MeOH (15 mL) at ambient temperature for 45 min, were added in portions of 1 mL and the solution was stirred at ambient temperature for 1 h. The solvent was removed on a rotary evaporator, the residue extracted with dichloromethane, the solution filtered and the solvent removed on a rotary evaporator. The residue was dissolved in warm acetone and the solution concentrated on a rotary evaporator until precipitation occurred, at which point diethyl ether was added and the solution was stored at 253 K. The orange product was collected by filtration and dried in air. Yield: 174.7 mg (66%); ^{1}H NMR ($CDCl_3$): δ = 7.55 (d, J = 5 Hz, 1H), 6.51 (d, J = 5 Hz, 1H), 5.54 (d, J = 5.5 Hz, 1H), 5.51 (d, J = 5.5 Hz, 1H), 5.32 (d, J = 5.5 Hz, 1H), 5.28 (d, J = 5.5 Hz, 1H), 2.92 (sept, J = 7 Hz, 1H), 2.42 (s, 3H), 2.33 (s, 1H), 1.34 (d, J = 7 Hz, 3H), 1.31 ppm (d, J = 7 Hz, 3H); elemental analysis calcd (%) for $C_{16}H_{19}ClO_3Ru$ (395.84): C 48.55, H 4.84; found: C 48.61, H 4.62. X-ray-diffraction-quality crystals were grown from a solution containing complex **2** and excess NaCl in water in an NMR tube at ambient temperature over a period of 2 d.

[Os(η^6-*p*-cym)(mal)(9EtG)]PF$_6$ (7): A solution of **1** (58.7 mg, 0.12 mmol) and $AgPF_6$ (33.9 mg, 0.13 mmol, 1.1 mol equiv) in MeOH (1.5 mL) was stirred at ambient temperature for 2.5 h under argon, and the resulting AgCl precipitate removed by filtering the solution through a glass-wool plug. 9-EtG (22.4 mg, 0.13 mmol, 1 mol equiv) was added and the resulting mixture stirred at ambient temperature under argon for 20 h. The solvent volume was reduced and the orange product, which precipitated out on addition of diethyl ether, was recovered by filtration. It was washed with diethyl ether (10 mL) and air-dried. Yield: 70.4 mg (75%); ^{1}H NMR ([D$_4$]MeOD): δ = 7.86 (d, J = 5.3 Hz, 1H), 7.76 (s, 1H), 6.65 (d, J = 5.0 Hz, 1H), 6.30 (d, J = 5.5 Hz, 1H), 6.14 (d, J = 5.5 Hz, 1H), 6.04 (d, J = 5.3 Hz, 1H), 5.95 (d, J = 5.3 Hz, 1H), 4.09 (q, J = 7.1 Hz, 2H), 2.67 (sept, J = 7.1 Hz, 1H), 2.48 (s, 3H), 2.13 (s, 3H), 1.33 (d, J = 7.3 Hz, 3H), 1.30 (d, J = 7.1 Hz, 3H), 1.22 ppm (d, J = 7.1 Hz, 3H); ESI-MS: m/z: calcd for $C_{23}H_{28}N_5O_4Os$: 630.2; found: 630.5; elemental analysis calcd (%) for $C_{23}H_{28}F_6N_5O_4OsP$ (773.69): C 35.70, H 3.65, N 9.05; found: C 36.05, H 3.55, N 8.71.

X-ray crystallography: The diffraction data for complexes **1** and **2**·2H$_2$O were collected by using a Bruker (Siemens) Smart Apex CCD diffractometer equipped with an Oxford Cryosystems low-temperature device operating at 150 K. Absorption corrections were performed with the multiscan procedure SADABS.[39] The structures of **1** and **2**·2H$_2$O were solved by using direct methods (SIR92)[40] and Patterson methods (DIRDIF),[41] respectively, and refined against F^2 by using SHELXL-97.[42] Hydrogen atoms were located in a difference map, but placed in ideal positions and not refined. CCDC-603587 (**1**) and 603588 (**2**·2H$_2$O) contain the supplementary crystallographic data for this paper. These data can be obtained free of charge from the Cambridge Crystallographic Data Centre via www.ccdc.cam.ac.uk/data_request/cif.

NMR spectroscopy: ^{1}H NMR spectra were acquired on Bruker DPX 360 (^{1}H = 360 MHz), DMX 500 (^{1}H = 500 MHz), AVA 600 (^{1}H = 600 MHz) or AVA 800 (^{1}H = 800 MHz) spectrometers. ^{1}H NMR spectra in D_2O or 90% H_2O/10% D_2O were typically acquired with water suppression by the Shaka[43] or presaturation methods. ^{1}H NMR chemical shifts were internally referenced to 1,4-dioxane (3.75 ppm) for aqueous solutions, C*H*Cl$_3$ (7.26 ppm) for $CDCl_3$, MeO*H* (3.34 ppm) for [D$_4$]MeOD and toluene (7.09 ppm) for [D$_8$]toluene solutions. All data processing was carried out by using XWIN-NMR version 3.6 (Bruker, UK).

Mass spectrometry: ESI mass spectra were obtained on a Micromass Platform II mass spectrometer and D_2O/H_2O solutions were infused directly. The capillary voltage was 3.5 V and the cone voltage was varied between 20 and 50 V. The source temperature was 353 K. Mass spectra were recorded with a scan range m/z: 200 to 1200 for positive ions.

pH measurement: pH values of aqueous (90% H_2O/10% D_2O) NMR samples were measured at approximately 298 K directly in the NMR tube, before and after recording NMR spectra, by using a Corning 145 pH meter equipped with a micro combination electrode calibrated with Aldrich buffer solutions at pH 4, 7 and 10, without correction for effects of D on the glass electrode. pH meter readings for D_2O solutions are termed pH*.

Cytotoxicity: Cytotoxicity assays on human A549 lung and A2780 ovarian cancer cells were performed as reported previously.[10]

Reactions under biological test conditions: Samples were prepared so as to mimic typical biological test conditions (concentrations and solvents). A 50 μM stock solution of **1** in 0.125% [D$_6$]DMSO/99.875% D_2O (v/v) (measured pH* 6.87) was prepared by dissolution of **1** in [D$_6$]DMSO followed by rapid dilution with D_2O. An aliquot of this stock solution was then diluted with D_2O to give a 2 μM Os solution (measured pH* 7.28). ^{1}H NMR spectra (800 MHz) were recorded after approximately 10 min at 298 K. Samples were then incubated at 310 K for 24 h (a typical cell exposure time and temperature) and ^{1}H NMR spectra were recorded at 310 K. Samples were also prepared in the absence of [D$_6$]DMSO. Samples at 8 and 200 μM were prepared in a similar manner, but the D_2O was replaced with 100 mM NaCl in D_2O.

Stability of Os and Ru O,O-chelated complexes: Stock solutions (2 mM) of the complexes **1**, **2**, **11** or **12** were prepared in D_2O, sonicated for approximately 10 min and filtered through a glass-wool plug. Solutions at 1000, 500, 250, 100, 50 and 20 μM were prepared from this stock solution and D_2O. Samples were incubated at 310 K (24 h) before addition of dioxane as internal standard, the pH* values (≈6–7.5) were measured and the ^{1}H NMR spectra recorded at 298 K. ESI mass spectra were obtained from 50 μM solutions of Ru complexes **2** and **12**.

To determine the binding constants of 9-EtG adducts, a 2 mM stock solution of complex **7** was prepared in D_2O, sonicated for approximately 10 min and filtered through a glass-wool plug. Solutions at 1000, 500, 250, 100, 50 and 20 μM were prepared from this stock solution and D_2O, dioxane was added as an internal standard, and the ^{1}H NMR spectra were recorded at 298 K. Complexes **7** and **8** were also prepared in situ by mixing equimolar solutions of **1** or **2** and 9-EtG in D_2O to give final concentrations of 1000, 500, 250, 100, 50 and 20 μM. Dioxane was added as an internal reference and the ^{1}H NMR spectra recorded (298 K). Equilibrium constants for formation of the 9-EtG adducts of the aqua complexes were obtained from the slopes of plots of [bound complex **7**/**8**]/[free 9-EtG] versus [unbound aqua complex **1a**/**2a**], based on integration of ^{1}H NMR spectroscopic peaks. These data were collected before the second equilibrium, involving hydroxo-bridged dimer formation, contributed.

Dynamic NMR spectroscopic studies: The ^{1}H NMR spectrum of a solution of **1** (10 mM) in [D$_4$]MeOD was recorded at 223 K and then at 10 K increments up to 323 K on a Bruker DMX 360 NMR spectrometer.

Computational studies: DFT calculations were carried out by using the Amsterdam density functional (ADF) program suite version 2005.01.[44] Geometries and energies were obtained by using the Perdew–Wang gradient-corrected functional (PW91) with scalar ZORA relativistic corrections.[45–49] The frozen-core approximation[50] (core small keyword) was applied by using triple-ζ plus polarisation (TZP) bases. Default convergence criteria were applied for self-consistent field (SCF) and geometry optimisation, except that the angle threshold was set to 1.5° for transition-state (TS) searches and 2.5° otherwise. The criteria were relaxed due to the long bond lengths at the TSs, which make it harder to define accurately the torsional terms. The same problem occurred for reactant and product species, as the respective entering and leaving groups are included in the calculation and their relatively weak interaction with the rest of

the complex again leads to less well-defined torsional terms. However, the energetic consequences of relaxing the angle constraints are negligible. ADF reported a single negative eigenvalue in the Hessian matrix for all TS optimisations. TSs were not confirmed with frequency calculations. The COSMO as implemented in ADF was used to simulate the aqueous environment with $\varepsilon = 80$ and probe radius = 1.4 Å. The atomic radii (Å) used were: Os = 2.120, O = 1.72, C = 1.4, N = 1.5, H = 1.16, Cl = 2.00.

Acknowledgements

We thank Oncosense Ltd, the EPSRC and the University of Edinburgh (studentships for A.F.A.P. and M.M.) for support, members of EC COST Group D20 for stimulating discussions, John Miller for assistance with variable-temperature NMR, Emily Jones and Daniel Cole for some cell tests and Rhona E. Aird and Duncan I. Jodrell for advice and assistance with cell culture.

[1] a) M. L. Tobe, J. Burgess, *Inorganic Reaction Mechanisms*, Addison Wesley Longman, Essex, **1999**, pp. 173–174; b) D. F. Shriver, P. W. Atkins, *Inorganic Chemistry*, 3rd ed., Oxford University Press, Oxford, **1999**, p. 245; c) P. A. Lay, W. D. Harman, *Adv. Inorg. Chem.* **1991**, *37*, 219–379; d) D. T. Richens, *The Chemistry of Aqua Ions*, Wiley, Chichester, **1997**, pp. 421–429; e) W. P. Griffith in *Comprehensive Coordination Chemistry, Vol. 4* (Ed.: G. Wilkinson), Pergamon, Oxford, **1987**, pp. 519–633; f) M. T. Ashby, S. S. Alguindigue, M. A. Khan, *Organometallics* **2000**, *19*, 547–552; g) R. George, J. M. Andersen, J. R. Moss, *J. Organomet. Chem.* **1995**, *505*, 131–133; h) J. Halpern, L. Cai, P. J. Desrosiers, Z. Lin, *J. Chem. Soc. Dalton Trans.* **1991**, 717–723.

[2] R. E. Aird, J. Cummings, A. A. Ritchie, M. Muir, R. E. Morris, H. Chen, P. J. Sadler, D. I. Jodrell, *Br. J. Cancer* **2002**, *86*, 1652–1657.

[3] R. E. Morris, R. E. Aird, P. del S. Murdoch, H. Chen, J. Cummings, N. D. Hughes, S. Parsons, A. Parkin, G. Boyd, D. I. Jodrell, P. J. Sadler, *J. Med. Chem.* **2001**, *44*, 3616–3621.

[4] A. Habtemariam, M. Melchart, R. Fernández, S. Parsons, I. Oswald, A. Parkin, F. P. A. Fabbiani, J. Davidson, A. Dawson, R. E. Aird, D. I. Jodrell, P. J. Sadler, *J. Med. Chem.* **2006**, *49*, 6858–6868.

[5] Y. K. Yan, M. Melchart, A. Habtemariam, P. J. Sadler, *Chem. Commun.* **2005**, *38*, 4764–4776.

[6] M. Melchart, P. J. Sadler in *Bioorganometallics, Vol. 1* (Ed.: G. Jaouen), Wiley-VCH, Weinheim, **2006**, pp. 39–64.

[7] Y. Hung, W. Kung, H. Taube, *Inorg. Chem.* **1981**, *20*, 457–463.

[8] M. Stebler-Röthlisberger, W. Hummel, P. A. Pittet, H. B. Bürgi, A. Ludi, A. E. Merbach, *Inorg. Chem.* **1988**, *27*, 1358–1363.

[9] H. D. Mui, J. L. Brumaghim, C. L. Gross, G. S. Girolami, *Organometallics* **1999**, *18*, 3264–3272.

[10] A. F. A. Peacock, A. Habtemariam, R. Fernández, V. Walland, F. P. A. Fabbiani, S. Parsons, R. E. Aird, D. I. Jodrell, P. J. Sadler, *J. Am. Chem. Soc.* **2006**, *128*, 1739–1748.

[11] R. Fernández, M. Melchart, A. Habtemariam, S. Parsons, P. J. Sadler *Chem. Eur. J.* **2004**, *10*, 5173–5179.

[12] M. Hironishi, R. Kordek, R. Yanagihara, R. M. Garruto, *Neurodegeneration* **1996**, *5*, 325–329.

[13] K. H. Thompson, C. A. Barta, C. Orvig, *Chem. Soc. Rev.* **2006**, *35*, 545–556.

[14] M. Melchior, S. J. Rettig, B. D. Liboiron, K. Thompson, V. G. Yuen, J. H. McNeill, C. Orvig, *Inorg. Chem.* **2001**, *40*, 4686–4690.

[15] S. Verma, M. C. Cam, J. H. McNeill, *J. Am. Coll. Nutr.* **1998**, *17*, 11–18.

[16] C. D. Katsetos, J. Savory, M. M. Herman, R. M. Carpenter, A. Frankfurter, C. D. Hewitt, M. R. Willis, *Neuropathol. Appl. Neurobiol.* **1990**, *16*, 511–528.

[17] M. A. Jakupec, B. K. Keppler, *Met. Ions Biol. Syst.* **2004**, *42*, 425–462.

[18] M. M. Finnegan, T. G. Lutz, W. O. Nelson, A. Smith, C. Orvig, *Inorg. Chem.* **1987**, *26*, 2171–2176.

[19] M. T. Ahmet, C. S. Frampton, J. Silver, *J. Chem. Soc. Dalton Trans.* **1988**, 1159–1163.

[20] R. S. Harvey, D. M. Reffitt, L. A. Doig, J. Meenan, R. D. Ellis, R. P. H. Thompson, J. J. Powell, *Aliment. Pharmacol. Ther.* **1998**, *12*, 845–848.

[21] L. Carter, D. L. Davies, J. Fawcett, D. R. Russell, *Polyhedron* **1993**, *12*, 1599–1602.

[22] G. Capper, L. C. Carter, D. L. Davies, J. Fawcett, D. R. Russell, *J. Chem. Soc. Dalton Trans.* **1996**, 1399–1403.

[23] R. Lang, K. Polborn, T. Severin, K. Severin, *Inorg. Chim. Acta* **1999**, *294*, 62–67.

[24] Z. Grote, R. Scopelliti, K. J. Severin, *J. Am. Chem. Soc.* **2004**, *126*, 16959–16972.

[25] J. P. Perdew, Y. Wang, *Phys. Rev. B Condens. Matter* **1992**, *45*, 13244–13249.

[26] For a conductorlike screening model see: a) A. Klamt, G. Schüürmann, *J. Chem. Soc. Perkin Trans. 2* **1993**, 799–805; b) A. Klamt, *J. Phys. Chem.* **1995**, *99*, 2224–2235; c) A. Klamt, V. Jones, *J. Chem. Phys.* **1996**, *105*, 9972–9981.

[27] IC_{50} values for cisplatin are 2.6 and 0.5 μM against the human A549 lung and A2780 ovarian cancer cells, respectively. S. M. Guichard, R. Else, E. Reid, B. Zeitlin, R. Aird, M. Muir, M. Dodds, H. Fiebig, P. J. Sadler, D. I. Jodrell, *Biochem. Pharmacol.* **2006**, *71*, 408–415.

[28] F. Wang, A. Habtemariam, E. P. L. van der Geer, R. Fernandez, M. Melchart, R. J. Deeth, R. Aird, S. Guichard, F. P. A. Fabbiani, P. Lozano-Casal, I. D. H. Oswald, D. I. Jodrell, S. Parsons, P. J. Sadler, *Proc. Natl. Acad. Sci. USA* **2005**, *102*, 18269–18274.

[29] A. P. Abbott, G. Capper, D. L. Davies, J. Fawcett, D. R. Russell, *J. Chem. Soc. Dalton Trans.* **1995**, 3709–3713.

[30] F. Wang, H. Chen, S. Parsons, I. D. H. Oswald, J. E. Davidson, P. J. Sadler, *Chem. Eur. J.* **2003**, *9*, 5810–5820.

[31] N. K. Dutt, S. Rahut, *J. Inorg. Nucl. Chem.* **1970**, *32*, 1035–1038.

[32] C. X. Zhang, S. J. Lippard, *Curr. Opin. Chem. Biol.* **2003**, *7*, 481–489.

[33] V. Brabec, *Prog. Nucleic Acid Res. Mol. Biol.* **2002**, *71*, 1–68.

[34] A. Frodl, D. Herebian, W. Sheldrick, *J. Chem. Soc. Dalton Trans.* **2002**, *19*, 3664–3673.

[35] O. Novakova, O. Vrana, V. I. Kiseleva, V. Brabec, *Eur. J. Biochem.* **1995**, *228*, 616–624.

[36] D. Lindow, C. Cortez, R. Harvey, *J. Am. Chem. Soc.* **1972**, *94*, 5406–5412.

[37] S. Stahl, H. Werner, *Organometallics* **1990**, *9*, 1876–1881.

[38] M. A. Bennett, A. K. Smith, *J. Chem. Soc. Dalton Trans.* **1974**, 233–241.

[39] SADABS: area-detector absorption correction; Siemens Industrial Automation, Madison, WI, **1996**.

[40] A. Altomare, G. Cascarano, G. Giacovazzo, A. Guagliardi, M. C. Burla, G. Polidori, M. Camalli, *J. Appl. Crystallogr.* **1994**, *27*, 435–435.

[41] P. T. Beurskens, G. Beurskens, R. de Gelder, S. Carcia-Granda, R. O. Gould, R. Israel, J. M. M. Smits, **1999**, the DIRDIF-00 program system, Technical Report of the Crystallography Laboratory, University of Nijmegen, The Netherlands.

[42] G. M. Sheldrick, SHELXL-97. Program for the refinement of crystal structures, University of Göttingen, Göttingen (Germany), **1997**.

[43] T. L. Hwang, A. J. Shaka, *J. Magn. Reson. A* **1995**, *112*, 275–279.

[44] E. J. Baerends, A. Bérces, C. Bo, P. M. Boerrigter, L. Cavallo, L. Deng, R. M. Dickson, D. E. Ellis, L. Fan, T. H. Fischer, C. Fonseca Guerra, S. J. A. van Gisbergen, J. A. Groeneveld, O. V. Gritsenko, F. E. Harris, P. van den Hoek, H. Jacobsen, G. van Kessel, F. Kootstra, E. van Lenthe, V. P. Osinga, P. H. T. Philipsen, D. Post, C. C. Pye, W. Ravenek, P. Ros, P. R. T. Schipper, G. Schreckenbach, J. G. Snijders, M. Sola, D. Swerhone, G. te Velde, P. Vernooijs, L. Versluis, O. Visser, E. van Wezenbeek, G. Wiesenekker, S. K. Wolff, T. K. Woo, T. Ziegler in "ADF 2005.01", Vrije Universiteit, Amsterdam (The Netherlands) **2005**.

[45] E. van Lenthe, A. E. Ehlers, E. J. Baerends, *J. Chem. Phys.* **1999**, *110*, 8943–8953.

[46] E. van Lenthe, E. J. Baerends, J. G. Snijders, *J. Chem. Phys.* **1993**, *99*, 4597–4610.
[47] E. van Lenthe, E. J. Baerends, J. G. Snijders, *J. Chem. Phys.* **1994**, *101*, 9783–9792.
[48] E. van Lenthe, R. van Leeuwen, E. J. Baerends, J. G. Snijders, *Int. J. Quantum Chem.* **1996**, *57*, 281–293.
[49] E. van Lenthe, J. G. Snijders, E. J. Baerends, *J. Chem. Phys.* **1996**, *105*, 6505–6516.
[50] E. J. Baerends, D. E. Ellis, P. Ros, *Theor. Chim. Acta* **1972**, *27*, 339–354.

Received: June 9, 2006
Published online: January 2, 2007

